JOURNAL OF PROPULSION AND POWER
Vol. 18, No. 1, January–February 2002

Shock Fitting a Transonic Cascade Solution into an Inverse Design Technique

Jeffrey W. Yokota* and Adam J. Medd†
University of Alberta, Edmonton, Alberta T6G 2G8, Canada

We present a new Lagrangian-based shock-fitting technique for inversely designing transonic turbomachinery cascade geometries. This method, which consists of a two-dimensional flowfield integrator, a camberline generator, and a passage-averaged momentum/pressure boundary condition, generates a cascade geometry to match a prescribed flow turning distribution. A complex-lamellar flow decomposition is used, first to show how discontinuous geometries are created when one's total turning distribution is specified to be continuous and shock-generated entropy gradients are present and then to construct a shock-fitting treatment that actively modifies the specified turning distribution to counter this effect. Finally, numerical results are presented to illustrate that, with this new shock-fitting approach, our transonic cascades are both geometrically continuous and faithful to the prescribed flow turning distribution.

I. Introduction

WITH the increase in their accuracy and efficiency, numerical simulations are now being implemented into every aspect of the aerodynamic design process. In fact, whereas they were once used mainly for generating postmortem analyses of intermediate designs, numerical methods are now being used for both design optimization[1–3] and inverse design.[4–6]

Although inverse methods are often most efficient, they require one to specify loading or pressure distributions, which, without proper judgement, can lead to poorly performing designs. Target distributions are often specified without any prior knowledge of their appropriateness or ability to be actively modified throughout the inverse design procedure. Thus, design-optimization schemes have begun to attract a tremendous amount of attention. In these schemes, one examines a large design space in hopes of identifying the optimal solution to a given number of constraints and objective functions. Unfortunately, global optimums are not easily obtained without careful construction of the appropriate geometric constraints, adjoint equations, and objective functions.[7,8] In fact, Drela[9] has shown that, whereas a multipoint optimization is needed to control both design and off-design performances, geometries that have been optimized over multiple objective functions are often susceptible to small-scale irregularities of significant consequence in viscous and transonic flows. Thus, mixed inverse design/design optimization scheme are being developed to exploit the strengths of each of these approaches.[1,10,11]

With this work we present a new Lagrangian-based shock-fitting technique for inversely designing transonic turbomachinery cascade geometries. This technique, which is based on the inverse-design theories of Hawthorne et al.[4] and Tan et al.[12] in general, and Dang[5] in particular, could be described as a shock-based optimization method because it actively modifies a prescribed velocity distribution until a geometrically continuous blade shape is produced.

In Dang's method[5] a compressible finite volume scheme is used to construct the flow around a cascade whose geometry is designed to match a prescribed flow turning distribution. The cascade geometry is decomposed into a prescribed thickness distribution and a camberline, the shape of which is obtained, iteratively, from a no-flux boundary condition. The flowfield on which this no-flux condition is applied is governed by a passage-averaged momentum analysis that couples the cascade pressure boundary conditions to the prescribed flow turning distribution. This approach differs significantly from the more conventional inverse-design methods of Giles and Drela,[6] Leonard and Van den Braembussche,[13] or Tong and Thompkins.[14] In these schemes one is required to specify the pressure distributions along the blade's pressure and suction surfaces, and one has little opportunity to enforce such structural requirements as blade thickness. Furthermore, unlike Dang's[5] method, it can be difficult to extend these techniques to three dimensions because pressure distributions must be specified along streamlines whose paths are not easily anticipated.[15]

Classical techniques, such as the hodograph method, are capable of generating weak or shockless transonic designs,[16,17] whereas current methods, such as Dang's,[5] produce discontinuous cascade geometries in the presence of strong shocks.[18] We will show how a complex-lamellar decomposition of our flowfield, and its passage-averaged flow turning, can be used to derive a pressure boundary condition that ensures that our transonic designs are both geometrically continuous and faithful to the prescribed flow turning distribution. With this analysis we will first show how discontinuous geometries are created when one's total turning distribution is specified to be continuous and shock-generated entropy gradients are present. Then we will construct a shock-fitting treatment that actively modifies the specified turning distribution to counter this effect.

Finally, numerical results are presented to illustrate the utility of this inverse design technique and explore a number of different transonic designs, both geometrically continuous and discontinuous.

II. Governing Equations

An inverse design technique requires that we develop a coupled system of equations from which to obtain both the geometry of interest and the flowfield around it. This is in contrast to an analysis method in which the flow around a known geometry is constructed.

For an inviscid, compressible flow in the Cartesian coordinate system (x, y), the conservation laws of continuity, linear momentum, and energy can be written

$$\frac{\mathrm{D}}{\mathrm{D}t}(\rho J) = 0 \tag{1}$$

$$\frac{\mathrm{D}}{\mathrm{D}t}(\rho u_i J) = -J\frac{\partial p}{\partial x_i} \tag{2}$$

$$\frac{\mathrm{D}}{\mathrm{D}t}(\rho E J) = -J\frac{\partial}{\partial x_i}(p u_i) \tag{3}$$

Received 3 June 2000; revision received 26 December 2000; accepted for publication 27 January 2001.

*Associate Professor, Department of Mechanical Engineering. Senior Member AIAA.
†Graduate Student, Department of Mechanical Engineering.

where ρ is density, p is pressure, $u_i = (u, v)$ are Cartesian velocity components, E is the total energy, J is the transformation Jacobian between Lagrangian and Cartesian coordinates, and summation over repeated indices is assumed.

The cascade geometry can be defined as

$$\alpha^{\pm} = y - (f \pm T/2) \tag{4}$$

where α^+ and α^- are the blade's upper and lower surfaces, $f = f(x)$ is the blade's camber line, and $T = T(x)$ is the blade's thickness distribution. If we then assume that the blade surfaces are no-flux surfaces, we can write

$$\boldsymbol{u} \cdot \nabla \alpha^+ = \boldsymbol{u} \cdot \nabla \alpha^- = 0 \tag{5}$$

which, when combined with Eq. (4),[3] produces following equation for the camberline

$$\frac{(u^+ + u^-)}{2}\frac{\partial f}{\partial x} = -\frac{(u^+ + u^-)}{4}\frac{\mathrm{d}T}{\mathrm{d}x} + \frac{(v^+ + v^-)}{2} \tag{6}$$

where the Cartesian velocity components (u^+, u^-, v^+, and v^-) are obtained from the cascade's upper and lower surfaces, respectively.

III. Numerical Approximation

Whereas the camber line equation, Eq. (6), is discretized into a one-sided finite difference approximation that is solved algebraically, the flow equations (1–3) are combined into a single nonlinear system

$$\int \frac{\partial \boldsymbol{w}}{\partial t}\,\mathrm{d}\forall + \oint \bar{\bar{F}} \cdot \boldsymbol{n}\,\mathrm{d}\sigma = 0 \tag{7}$$

where $\boldsymbol{w} = \{\rho, \rho u, \rho v, \rho E\}$, $\bar{\bar{F}} \cdot \boldsymbol{e}_x = \{\rho u, \rho u^2 + p, \rho uv, u(E + p)\}$, $\boldsymbol{n}$ is a surface normal, and $\mathrm{d}\forall$ and $\mathrm{d}\sigma$ are elemental volumes and surface areas, respectively. This equation is then solved numerically by the second-order-accurate, four-stage multistage scheme of Jameson et al.[19] These equations are discretized by a finite volume formulation that approximates the spatial differences as a bilinearly averaged net flux across the faces of each mesh cell. Following the works of Jameson[20] and Pullium,[21] fourth-difference artificial dissipation terms are added throughout the flowfield to prevent odd–even decoupling of the numerical approximation, and second difference terms are added near shocks to prevent any undershooting or overshooting.

A. Solid-Wall Boundary Conditions

Along the blade surfaces, where t is a surface tangent, the following flux vectors must be constructed:

$$\boldsymbol{F} \cdot \boldsymbol{n}^{\pm} = \{\rho \boldsymbol{u} \cdot \boldsymbol{n},\ \rho(\boldsymbol{u} \cdot \boldsymbol{n})^2 + p,\ \rho(\boldsymbol{u} \cdot \boldsymbol{n})(\boldsymbol{u} \cdot \boldsymbol{t}),\ (\boldsymbol{u} \cdot \boldsymbol{n})(E + p)\}^{\pm} \tag{8}$$

In an analysis method, where the flow is being calculated around a fixed geometry, the normal velocities along the solid surfaces are set to

$$\boldsymbol{u} \cdot \boldsymbol{n} = 0 \tag{9}$$

whereas the surface pressures are extrapolated from the interior flowfield

$$p(f \pm T/2) = p(f \pm [T + \Delta n]/2) \mp \Delta p/2 \tag{10}$$

where Δn is the grid spacing in the direction normal to the solid surface and a zeroth-order extrapolation is produced by setting $\Delta p = 0$.

In an inverse-design method, where the geometry is not known a priori, one cannot impose Eq. (9) directly, but instead one allows the geometry to evolve until the no-flux condition is satisfied, implicitly, by Eq. (6). Thus, Cartesian velocities from the interior flowfield are extrapolated to the solid surfaces,

$$u(f \pm T/2) = u(f \pm [T + \Delta n]/2) \tag{11}$$

$$v(f \pm T/2) = v(f \pm [T + \Delta n]/2) \tag{12}$$

and pressures are constructed along the cascades upper and lower surfaces from a first-order Taylor series approximation,

$$p(f \pm T/2) = p(f) \pm \Delta p/2 \tag{13}$$

Here the pressures along the cascade's camberline are approximated by

$$p(f) = 0.5\{p(f + [T + \Delta n]/2) + p(f - [T + \Delta n]/2)\} \tag{14}$$

whereas the pressure difference across the cascade, in the pitchwise direction, is equated to the mass flow weighted flow turning distribution

$$\Delta p = \dot{m}\left.\frac{\mathrm{d}\bar{v}}{\mathrm{d}x}\right|_{\text{input}} \tag{15}$$

The loading distribution takes the form

$$\frac{\mathrm{d}\bar{v}}{\mathrm{d}x} = C x^a (1 - x)^b \tag{16}$$

where the value of C is chosen to generate a specified amount of total turning,[4] whereas the constants a and b are used to control the general shape of the loading distribution. More specifically, C is obtained by integrating the prescribed loading distribution from leading to trailing edge and then equating this result to the total turning. Thus,

$$\Delta v = C \int_{x=le}^{x=te} x^a (1 - x)^b\,\mathrm{d}x \tag{17}$$

where Δv is the total flow turning specified a priori.

B. Solid-Wall Boundary Conditions: Transonic Flow

Although the solid-wall boundary condition, Eq. (15), is applicable to all flows, the transonic designs that these flows produce may be impractical to use. Because this condition requires one to specify a given loading distribution, a continuous cascade geometry can only be obtained from a discontinuous loading distribution. Thus, without knowing the effects of the shock a priori, one has little chance of inversely designing a smooth geometry. In fact, by specifying a smooth loading distribution, one is attempting to design a discontinuous cascade geometry that will effectively cancel the shock with a corresponding expansion wave. Although these designs are interesting, they generate flows that are extremely complicated and unlikely to be realized within a viscous fluid. The boundary layer's momentum displacement produces a small, but influential, blockage that is likely to alter the location of the shock–expansion wave interaction and negate the effectiveness of this design. Thus, we have developed a new transonic solid-wall boundary condition that ensures that our designs will be geometrically continuous.

Combining the first and second laws of thermodynamics, we can write

$$\mathrm{d}p = \rho\,\mathrm{d}h - \rho\Theta\,\mathrm{d}s \tag{18}$$

where Θ is temperature, h is enthalpy, and s is entropy. This equation suggests that we modify our pressure boundary condition to account for entropy gradients within the flow. Thus, we first decompose our velocity field into two components, one isentropic and the other entropy generating, and then use this velocity decomposition to construct our new boundary condition. Following Yokota,[22,23] we multiply the linear momentum equation, Eq. (2), by the Cartesian/Lagrangian transformation matrix $\partial x_i/\partial X_j$, to produce the tensor equation

$$\frac{\mathrm{D}}{\mathrm{D}t}\left\{\rho u_i J \frac{\partial x_i}{\partial X_j}\right\} - \rho J \frac{\partial}{\partial X_j}\left\{\frac{u_i u_i}{2}\right\} = -J\frac{\partial p}{\partial X_j} \tag{19}$$

which can then be integrated as

$$\int \frac{\mathrm{D}}{\mathrm{D}t}\left\{\rho u_i J \frac{\partial x_i}{\partial X_j}\right\}\mathrm{d}t - \rho J \int \frac{\partial}{\partial X_j}\left\{\frac{u_i u_i}{2}\right\}\mathrm{d}t = -\int J\frac{\partial p}{\partial X_j}\mathrm{d}t \tag{20}$$

such that

$$u_i \frac{\partial x_i}{\partial X_j} - a_j = \frac{\partial}{\partial X_j}\int \frac{u_i u_i}{2}\mathrm{d}t - \int \frac{1}{\rho}\frac{\partial p}{\partial X_j}\mathrm{d}t \tag{21}$$

where a_j is a vector constant of integration dependent on the material coordinates (X, Y). Applying Eq. (18) to this tensor equation, we can write

$$u_i \frac{\partial x_i}{\partial X_j} - a_j = \frac{\partial}{\partial X_j}\int \left\{\frac{u_i u_i}{2} - h\right\}\mathrm{d}t + \int \Theta \frac{\partial s}{\partial X_j}\mathrm{d}t \tag{22}$$

By defining the following Weber transformations (see Ref. 24)

$$\frac{\mathrm{D}\phi}{\mathrm{D}t} = \frac{u_i u_i}{2} - h \tag{23}$$

$$\frac{\mathrm{D}\eta}{\mathrm{D}t} = \Theta \tag{24}$$

we can rewrite Eq. (22) as

$$u_i \frac{\partial x_i}{\partial X_j} - A_j = \frac{\partial \phi}{\partial X_j} + \eta\frac{\partial s}{\partial X_j} - \int \eta \frac{\partial}{\partial X_j}\left\{\frac{\mathrm{D}s}{\mathrm{D}t}\right\}\mathrm{d}t \tag{25}$$

where A_j is a vector constant of integration that satisfies

$$\frac{\mathrm{D}A_j}{\mathrm{D}t} = 0 \tag{26}$$

Given that an inviscid, nonconducting fluid implies

$$\frac{\mathrm{D}s}{\mathrm{D}t} = 0 \tag{27}$$

Eq. (25) becomes

$$u_i \frac{\partial x_i}{\partial X_j} = \frac{\partial \phi}{\partial X_j} + A_j + \eta\frac{\partial s}{\partial X_j} \tag{28}$$

which, when multiplied by $\partial X_J/\partial x_i$, produces the following complex-lamellar decomposition

$$u_i = \frac{\partial \phi}{\partial x_i} + A_j\frac{\partial X_j}{\partial x_i} + \eta\frac{\partial s}{\partial x_i} \tag{29}$$

Because the last term in Eq. (29) can only exist downstream of a shock, we can reinterpret this decomposition as

$$u_i = u_i^\circ + \eta\frac{\partial s}{\partial x_i} \tag{30}$$

where u_i° is the velocity field that would otherwise exist on its own in a shockless flow. Following Yokota,[25] we then substitute this velocity decomposition back into the linear momentum equation, to produce

$$\frac{\mathrm{D}u_i^\circ}{\mathrm{D}t} + \frac{\mathrm{D}\eta}{\mathrm{D}t}\frac{\partial s}{\partial x_i} + \eta\frac{\partial}{\partial x_i}\left\{\frac{\mathrm{D}s}{\mathrm{D}t}\right\} - \frac{\partial u_j}{\partial x_i}\left\{\eta\frac{\partial s}{\partial x_j}\right\} = -\frac{1}{\rho}\frac{\partial p}{\partial x_i} \tag{31}$$

or

$$\rho\frac{\mathrm{D}u_i^\circ}{\mathrm{D}t} + \rho\Theta\frac{\partial s}{\partial x_i} - \rho\frac{\partial u_j}{\partial x_i}\left\{\eta\frac{\partial s}{\partial x_j}\right\} = -\frac{\partial p}{\partial x_i} \tag{32}$$

Finally, integrating the y component of this momentum equation, we obtain the following pressure equation

$$\Delta p = \int_{f+T/2}^{f+S-T/2}\rho\frac{\mathrm{D}v^\circ}{\mathrm{D}t}\mathrm{d}y + \int_{f+T/2}^{f+S-T/2}\rho\Theta\frac{\partial s}{\partial y}\mathrm{d}y - \int_{f+T/2}^{f+S-T/2}\rho\frac{\partial u_j}{\partial y}\left\{\eta\frac{\partial s}{\partial x_j}\right\}\mathrm{d}y \tag{33}$$

which, for a steady flow, when coupled to our definition of a mass-flux weighted flow turning, becomes

$$\begin{aligned}\Delta p &= \dot{m}\frac{\mathrm{d}\bar{v}}{\mathrm{d}x}\\ &= \dot{m}\frac{\mathrm{d}\bar{v}^\circ}{\mathrm{d}x} + \int_{f+T/2}^{f+S-T/2}\rho\Theta\frac{\partial s}{\partial y}\mathrm{d}y - \int_{f+T/2}^{f+S-T/2}\rho\frac{\partial u_j}{\partial y}\left\{\eta\frac{\partial s}{\partial x_j}\right\}\mathrm{d}y\end{aligned} \tag{34}$$

Thus, our pressure condition requires that we prescribe either the total flow turning or its isentropic counterpart.

1. *Prescribed Total Flow Turning: Shock Capturing*

By choosing to prescribe a total turning distribution, one's cascade geometry will be designed to satisfy the following pressure condition:

$$\Delta p = \dot{m}\left.\frac{\mathrm{d}\bar{v}}{\mathrm{d}x}\right|_{\text{input}} \tag{35}$$

Although one might prescribe a continuous total turning distribution, it is obvious from Eq. (25) that the resulting cascade geometry need not be. In fact, a continuous total turning distribution requires that the effects of the entropy jump across the shock be canceled by an equal but opposite jump in the isentropic turning distribution. Thus, the resulting cascade geometry will also be discontinuous. Evidence of this behavior can be found in Dang's[5] and Dang and Isgro's[18] work where virtually all of the inversely designed supersonic blades are geometrically discontinuous.

2. *Prescribed Isentropic Flow Turning: Shock Fitting*

A continuous cascade geometry can be generated by first prescribing a continuous, isentropic turning distribution and then fitting the effects of the shock into our pressure condition. Thus, our pressure condition becomes

$$\Delta p = \dot{m}\left.\frac{\mathrm{d}\bar{v}^\circ}{\mathrm{d}x}\right|_{\text{input}} + \int_{f+T/2}^{f+S-T/2}\rho\Theta\frac{\partial s}{\partial y}\mathrm{d}y - \int_{f+T/2}^{f+S-T/2}\rho\frac{\partial u_j}{\partial y}\left\{\eta\frac{\partial s}{\partial x_j}\right\}\mathrm{d}y \tag{36}$$

Given that all of our calculations are performed on sheared H grids whose vertical grid lines are aligned with the y axis, we can invoke both the first law of thermodynamics

$$\Delta s = s_2 - s_1 = R\,\ell n\left|(p_2/p_1)^{1/(\gamma-1)}(\rho_1/\rho_2)^{\gamma/(\gamma-1)}\right| \tag{37}$$

and the trapezoidal rule to model the integrated entropy-gradient term as

$$\begin{aligned}\int_{f+T/2}^{f+S-T/2}\rho\Theta\frac{\partial s}{\partial y}\mathrm{d}y &\approx \int_{f+T/2}^{f+S-T/2}\rho\Theta\frac{\Delta s}{\Delta y}\mathrm{d}y\\ &\approx \sum_{j=2}^{n+1} p_j\,\ell n\left|\left(\frac{p_{j+\frac{1}{2}}}{p_{j-\frac{1}{2}}}\right)^{1/(\gamma-1)}\left(\frac{\rho_{j-\frac{1}{2}}}{\rho_{j+\frac{1}{2}}}\right)^{\gamma/(\gamma-1)}\right|\end{aligned} \tag{38}$$

where n is the number of mesh cells across the passage, the cell centers are indexed by the subscript j, and the subscripts $j+\frac{1}{2}$

identify the cell faces. The final term needed to be modeled is the integrated shock-induced velocity term

$$\int_{f+T/2}^{f+S-T/2} \rho \frac{\partial u_j}{\partial y} \left\{ \eta \frac{\partial s}{\partial x_j} \right\} \mathrm{d}y = \int_{f+T/2}^{f+S-T/2} \rho \left\{ u^s \frac{\partial u}{\partial y} + v^s \frac{\partial v}{\partial y} \right\} \mathrm{d}y \tag{39}$$

where u^s and v^s are the shock-induced velocity components that alter the otherwise isentropic turning distribution. Because the shock-induced velocity components can only exist in the presence of the entropy gradients, we model this integrated term as

$$\int_{f+T/2}^{f+S-T/2} \rho \frac{\partial u_j}{\partial y} \left\{ \eta \frac{\partial s}{\partial x_j} \right\} \mathrm{d}y \approx k_2 \sum_{j=2}^{n+1} p_j \ell n \left| \left(\frac{p_{j+\frac{1}{2}}}{p_{j-\frac{1}{2}}} \right)^{1/(\gamma-1)} \left(\frac{\rho_{j-\frac{1}{2}}}{\rho_{j+\frac{1}{2}}} \right)^{\gamma/(\gamma-1)} \right| \tag{40}$$

where the scalar constant $4 \le k_2 \le 6$ was determined empirically from several different test cases. Thus, for a transonic flow, our pressure boundary condition becomes

$$\Delta p = \dot{m} \frac{\mathrm{d}\bar{v}^\circ}{\mathrm{d}x}\bigg|_{\text{input}} + (1-k_2) \sum_{j=2}^{n+1} p_j \ell n \left| \left(\frac{p_{j+\frac{1}{2}}}{p_{j-\frac{1}{2}}} \right)^{1/(\gamma-1)} \left(\frac{\rho_{j-\frac{1}{2}}}{\rho_{j+\frac{1}{2}}} \right)^{\gamma/(\gamma-1)} \right| \tag{41}$$

which allows us to inversely design a cascade whose geometry is both continuous and faithful to the prescribed flow turning distribution upstream of the shock.

Note that because a viscous flow can also be described by a complex-lamellar decomposition (Yokota[25,26]), these boundary conditions could also be used to model the effects of the boundary-layer-generated entropy. Thus, for a viscous design, we would treat the entropy term as either a modeled body force[27] or as the target variable to be minimized by an optimization scheme.

Because our current calculations are only inviscid, we need not worry about boundary-layer-generated entropy. However, we do need to avoid the small layer of entropy generated by the explicitly added artificial dissipation. Thus, to avoid including the effects of the artificial dissipation, the numerical implementation of Eq. (41) requires that the summation of the entropy terms occurs a couple of mesh cells away from the solid surfaces.

IV. Results

Numerical results are presented to illustrate the utility of this new inverse design technique and are compared to what would otherwise be obtained from Dang's original method.[5]

All of our calculations were two-dimensional and performed on sheared H-type meshes whose vertical grid lines were aligned with the y axis. Although the solutions produced on a body-fitted grid are often more accurate, pitchwise treatments are more easily constructed on a sheared H-type meshes[28,29] and are, therefore, the grids of choice for Dang's,[5] the Dang et al.,[15] and Dang and Isgro's[18] inverse-design method. The numerical domain, typically a 128×32 cell grid, was extended one chord upstream and downstream of the cascade's leading and training edges, respectively. Grid lines were clustered near the leading and trailing edges with an algebraic stretching that placed the smallest mesh cells, a size of approximately 0.004 of a chord, adjacent to the cascade's solid surfaces. A grid resolution study revealed that second-order-accurate, grid-independent results could be obtained from grids whose bladed regions contained a minimum of 64 mesh cells from leading to trailing edges, provided the specified turning distribution was also defined by more than double this number of points. These results showed that accuracy and grid independence were influenced more significantly by the construction of the specified turning distribution than by the actual grids themselves. Thus, our grids were constructed with 64 mesh cells between the leading and trailing edge and 32 mesh cells upstream and downstream of the bladed region. Both the thickness and turning distributions were specified by 161 data points that were then interpolated onto the bladed region's 64 mesh cells with a third-order-accurate Taylor series approximation. All calculations were run in double precision and converged to machine zero on 64-bit UNIX workstations from several different manufacturers.[30]

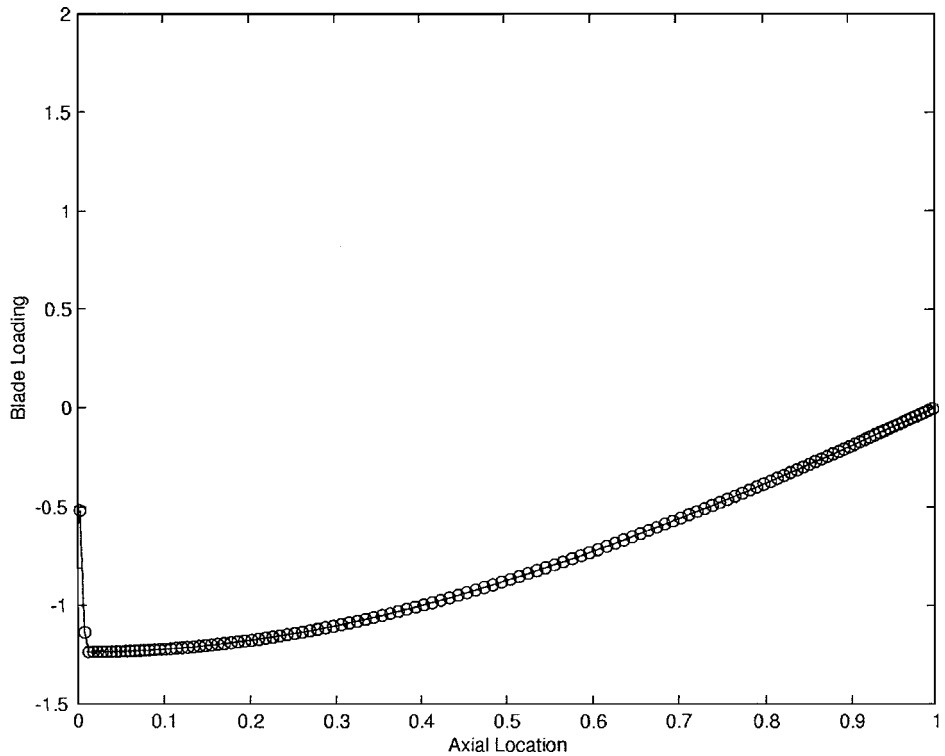

Fig. 1 Specified turning distribution: shock capturing.

Our first test case was a transonic cascade designed to produce a mass flow of $\dot{m} = 0.0.253 p_0 c/\sqrt{(RT_0)}$ for specified back pressure of $p = 0.65 p_0$. This cascade was designed by specifying a spacing-to-chord ratio of $S/c = 0.55$, a total flow turning of $\Delta\bar{v} = -0.783\sqrt{(RT_0)}$, and a flow turning distribution (Fig. 1) of the form

$$\frac{\mathrm{d}\bar{v}}{\mathrm{d}x} = C\cos\left(\frac{\pi - x}{2}\right) \tag{42}$$

The scalar constant C was again obtained from Eq. (17) and the specified total turning. Here the flow was turned approximately 33 deg from the inflow angle.

Flow calculations were performed on a 192×32 cell grid (128 cells between the leading and trailing edges) where once again the smallest cells, a size of approximately 0.002 of a chord, were found adjacent to the cascade's solid surfaces. The specified thickness distribution was of the form

$$T(x) = kx^{\frac{1}{2}}(1 - x)^{\frac{1}{2}} \tag{43}$$

where the scalar constant k is chosen to ensure that $T_{\max} = 0.3c$. The resulting transonic flow, which has a strong passage shock extending from the suction side of one cascade to the pressure side of the other, is shown to have accelerated the flow from an inflow

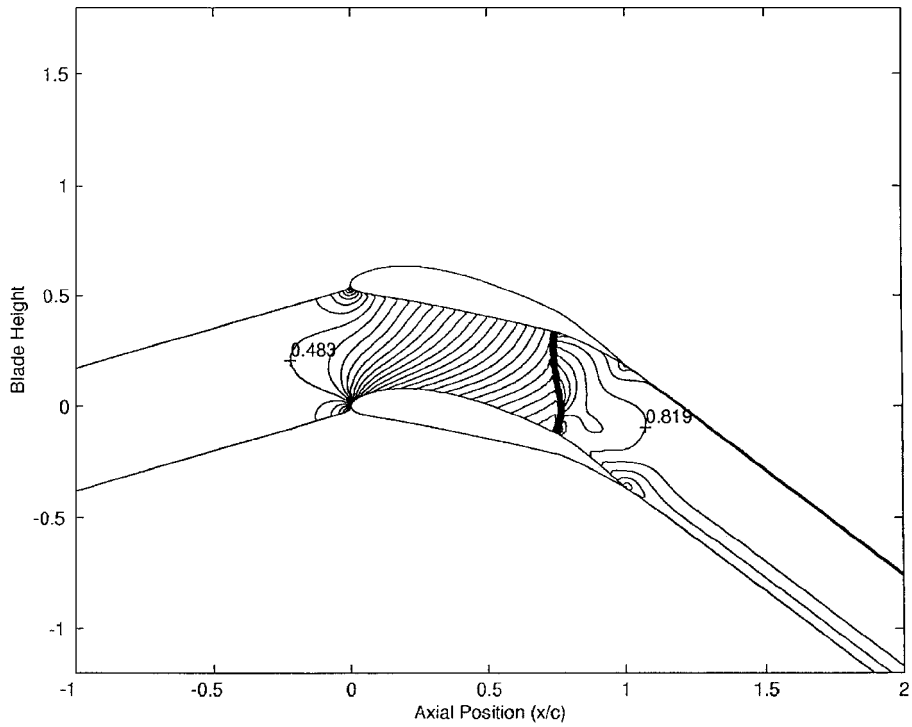

Fig. 2 Mach number field: shock capturing.

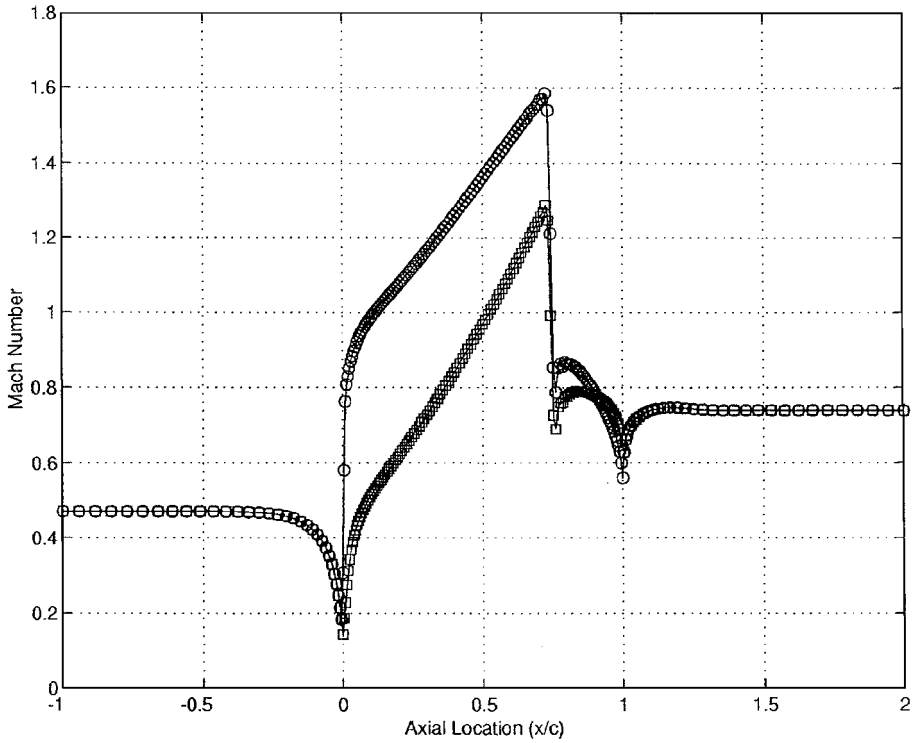

Fig. 3 Mach number distribution along the blade surfaces: shock capturing.

Mach number of approximately $M = 0.48$ to a downstream value of $M = 0.82$ (Fig. 2). The Mach number along the cascade's upper and lower surfaces can be seen in Fig. 3 where, at the maximum Mach number of approximately $M = 1.6$, the flow along the suction surface was suddenly decelerated, through a shock, to a Mach number of $M = 0.8$. The shock on the pressure surface occurs at the same axial location as its suction surface counterpart and drops the flow from a Mach number of $M = 1.3$ down to a Mach number of $M = 0.7$.

From these results we can see the discontinuous cascade geometry (Fig. 4) that results from specifying a continuous total turning distribution. Occurring immediately downstream of the passage shock is a cascade discontinuity that generates the flow expansion required to counteract the sudden compression. It is in this manner that a discontinuous cascade geometry produces a continuous total turning distribution. These results, obtained from Dang's original scheme,[5] are clearly unaffected by the presence of the explicitly added artificial dissipation that is needed to stabilize the flow near shocks without weakening them appreciably. Equation (34) shows that, by specifying a continuous overall flow turning distribution, one allows sharp entropy gradients to force the isentropic flow turning to

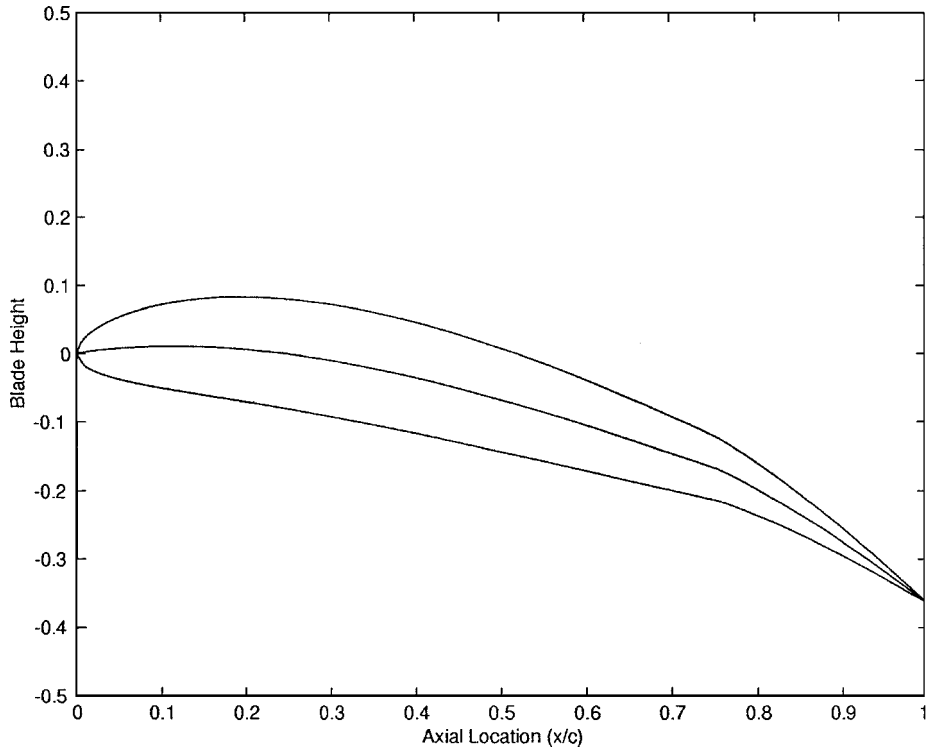

Fig. 4 Discontinuous blade geometry: shock capturing.

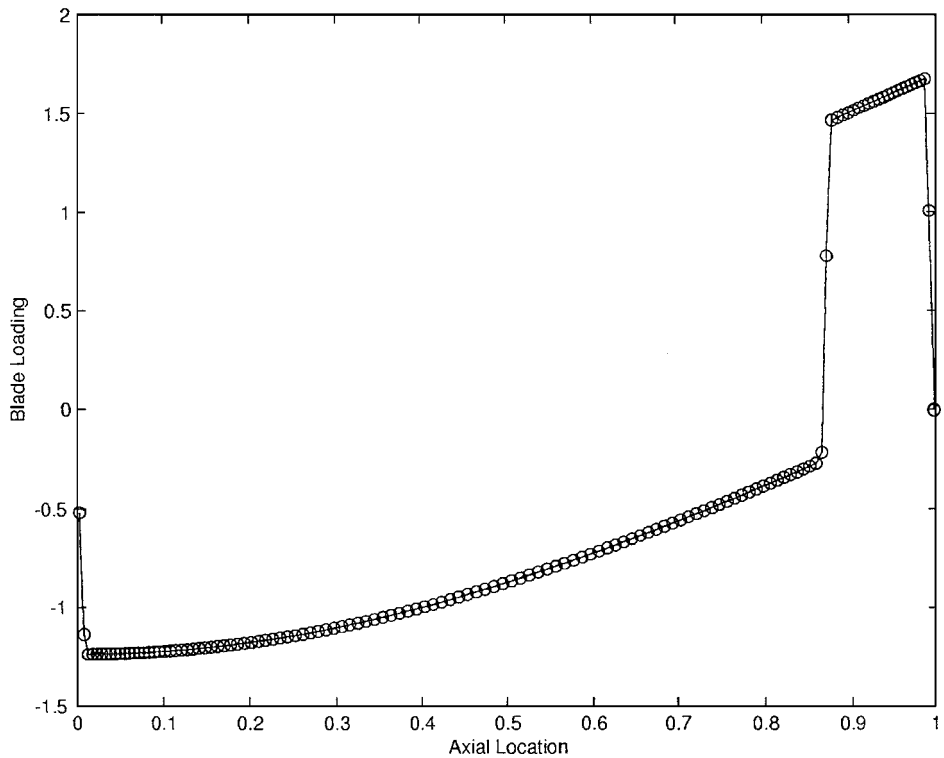

Fig. 5 Specified turning distribution: shock fitting.

be likewise, thus generating the discontinuous blade geometry. Unfortunately, viscous effects are likely to render these inviscid results physically unrealizable. The boundary layer's momentum displacement produces a small, but influential, blockage that is sure to alter the location of the shock–expansion wave interaction and negate the effectiveness of this design. An inability to cancel the shock is likely to result in an unanticipated shock-induced boundary-layer separation occurring prematurely along the blade's chord length. Although shock-induced boundary-layer separations are ofen inevitable, one would hope to isolate them to within the last 10 percent of the blades' chord length. Furthermore, an uncanceled shock is likely to generate a cove separation along the blade's pressure side that is capable of trapping hot gases from an upstream combustion chamber.

To avoid the cascade discontinuity of Fig. 4, we turn to the shock-fitting treatment of Sec. III.B.2. Here we prescribe a continuous, isentropic flow turning distribution (Fig. 1) and then fit the effects of the shock into our pressure condition, Eq. (41), using the scalar constant $k_2 = 5$. Here our shock velocity term is modeled as a function of the total entropy generated across the passage shock to produce the prescribed flow turning distribution shown in Fig. 5. This

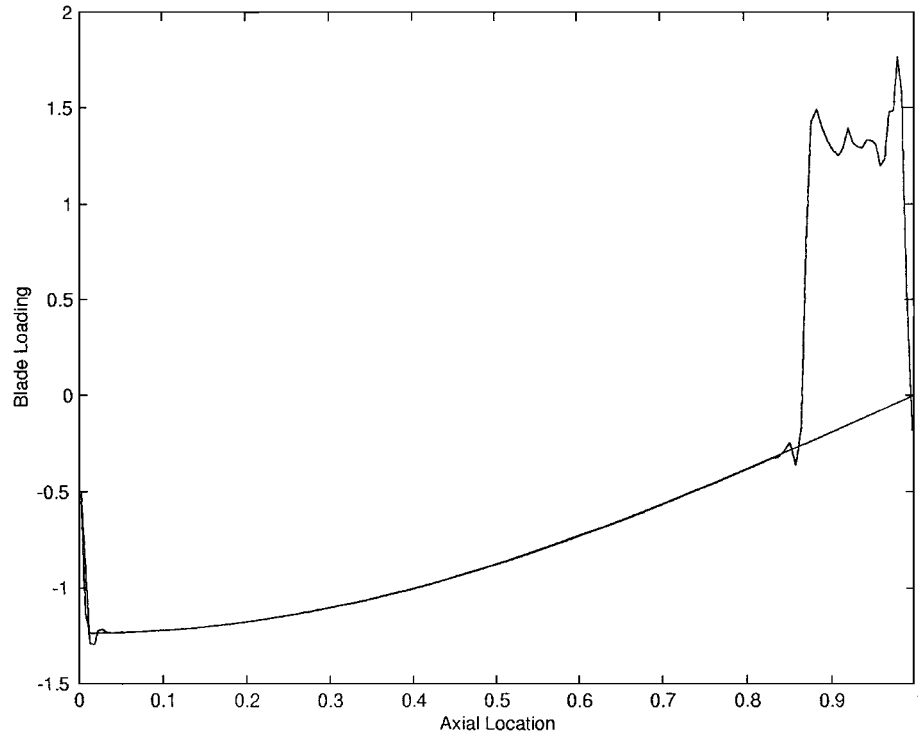

Fig. 6 Actual turning distribution: shock fitting.

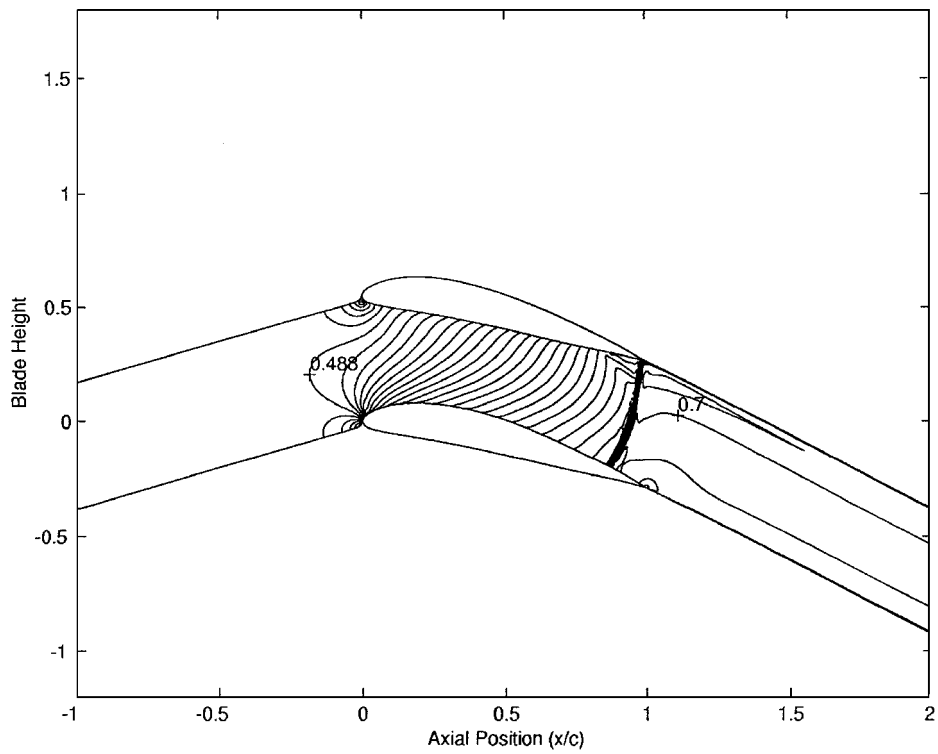

Fig. 7 Mach number field: shock fitting.

flow turning distribution is used to construct our pressure boundary conditions, and the actual flow turning that results can be seen in Fig. 6. The differences between the specified and calculated flow turning distributions occur downstream of the passage shock where our calculations have been modified by the entropy that has been created. However, upstream of the shock, this flowfield (Fig. 7) is identical to that of Fig. 2. Downstream of the passage shock our new flow turning distribution is responsible for generating a continuous cascade shape (Fig. 8) that moves the shock downstream toward the trailing edge of the pressure surface. The Mach number along the cascade's upper and lower surfaces can be seen in Fig. 9 where an maximum Mach number of approximately $M = 1.7$ was produced along the upper surface before it was suddenly decelerated, through the shock, to a Mach number of $M = 0.6$. The shock on the pressure surface occurs at the trailing edge and drops the flow from a Mach number of $M = 1.4$ down to a Mach number of $M = 0.6$. Whereas the passage shock is actually stronger within this continuous geometry, its position has moved significantly downstream toward the

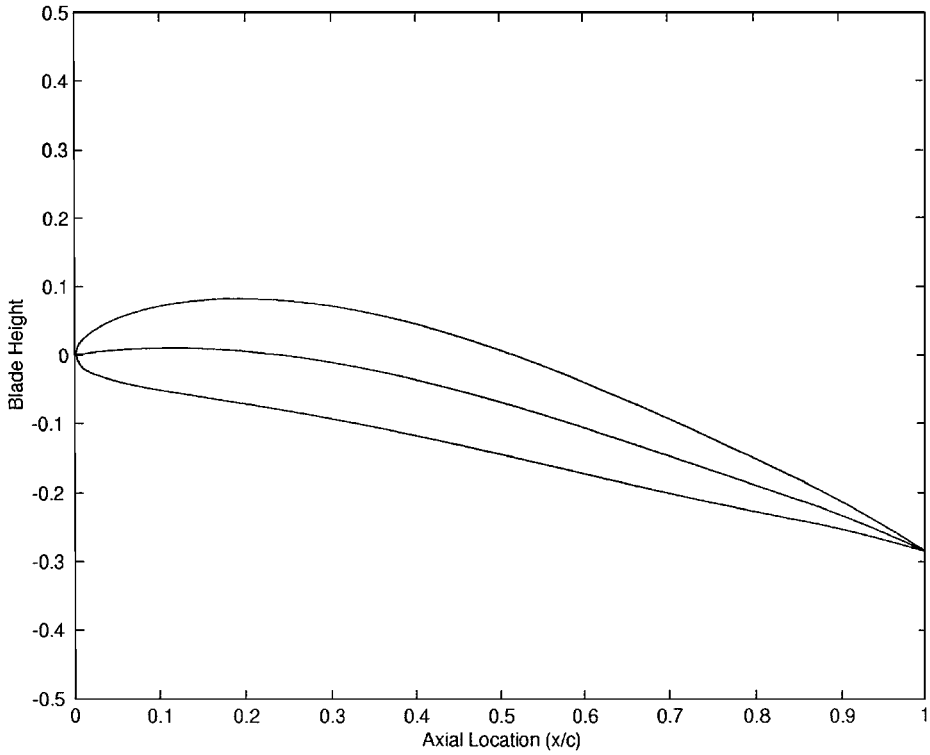

Fig. 8 Continuous blade geometry: shock fitting.

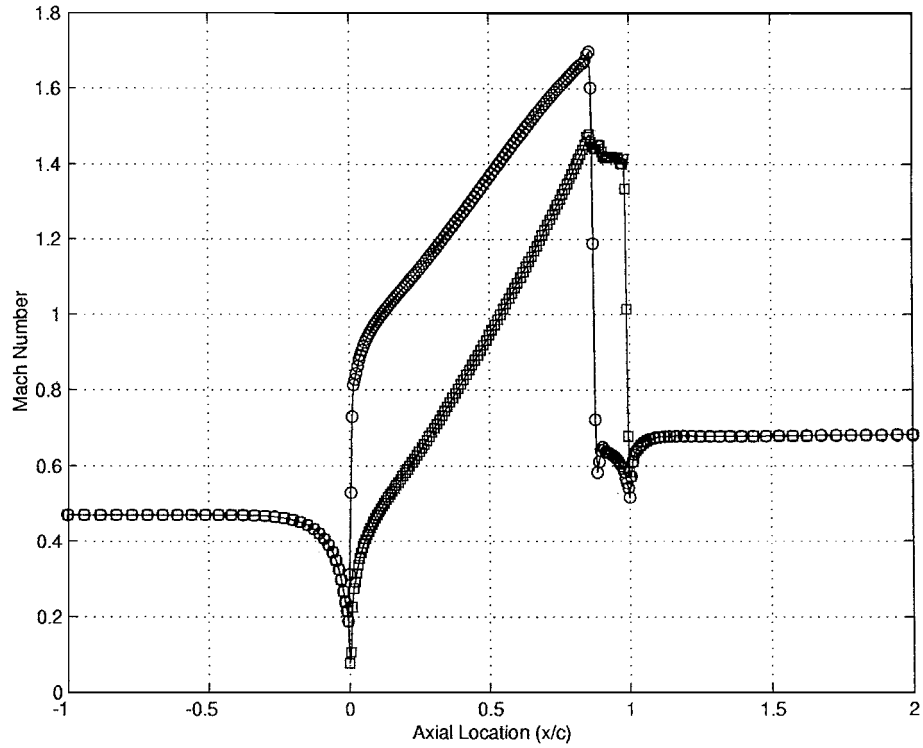

Fig. 9 Mach number distribution along the blade surfaces: shock fitting.

trailing edge. Along the suction surface the shock has moved from the 75 percent to 80 percent axial chord location, while the shock on the pressure surface has been pushed from the 75 percent axial chord location to the trailing edge—thus eliminating any chance of a shock-induced boundary-layer separation occuring along the pressure surface.

Clearly, these results show that our new flow turning/pressure boundary condition Eq. (32) ensures that our cascades are both geometrically continuous and faithful to the prescribed flow turning.

V. Conclusions

With this work we have presented a new Lagrangian-based shock-fitting technique for inversely designing turbomachinery cascade geometries in general and transonic ones in particular. This method, which consists of a two-dimensional flowfield integrator, a camberline generator, and a passage-averaged momentum/pressure boundary condition, generates a cascade geometry in response to a prescribed flow turning distribution.

A complex-lamellar flow decomposition was used to first show how discontinuous geometries are created when one's total turning distribution is specified to be continuous and shock-generated entropy gradients are present and then to construct a shock-fitting treatment that actively modifies the specified turning distribution to counter this effect.

Finally, numerical results were presented to illustrate that, with this new shock-fitting approach, our transonic cascades are both geometrically continuous and faithful to the prescribed flow turning distribution.

Acknowledgments

We are grateful to the Natural Sciences and Engineering Research Council of Canada (NSERC) for supporting this work under NSERC Grant OGP 170377. It is with pleasure that we also acknowledge the numerous conversations held throughout the course of this work with T. Q. Dang and his inverse-design code on which our work is based.

References

[1]Jameson, A., "Reengineering the Design Process Through Computation," *Journal of Aircraft*, Vol. 36, No. 1, 1999, pp. 36–50.

[2]Pironneau, O., "Optimal Shape Design for Aerodynamics," *Optimum Design Methods in Aerodynamics*, von Kármán Inst. for Fluid Dynamics, AGARD-VKI Lecture Series, Rhodes Saint Genese, Belgium, 1994.

[3]Elliot, J., and Peraire, J., "Practical Three-Dimensional Aerodynamic Design and Optimization Using Unstructured Meshes," *AIAA Journal*, Vol. 35, No. 9, 1997, pp. 1479–1485.

[4]Hawthorne, W. R., Wang, C., Tan, C. S., and McCune, J. E., "Theory of Blade Design for Large Deflections, Part 1: Two-Dimensional Cascades," *Journal of Engineering for Gas Turbines and Power*, Vol. 106, No. 2, 1984, pp. 346–353.

[5]Dang, T. Q., "Inverse Method for Turbomachinery Blades Using Shock-Capturing Techniques," AIAA Paper 95-2465, 1995.

[6]Giles, M. B., and Drela, M., "Two-Dimensional Transonic Aerodynamic Design Method," *AIAA Journal*, Vol. 25, No. 9, 1987, pp. 1199–1205.

[7]Sharatchandra, M. C., Sen, M., and Gad-el-Hak, M., "New Approach to Constrained Shape Optimization Using Genetic Algorithms," *AIAA Journal*, Vol. 36, No. 1, 1998, pp. 51–61.

[8]Arian, E., and Salas, M. D., "Admitting the Inadmissible: Adjoint Formulation for Incomplete Cost Functionals in Aerodynamic Design," *AIAA Journal*, Vol. 37, No. 1, 1999, pp. 37–44.

[9]Drela, M., "The Pros and Cons of Airfoil Optimization," *Frontiers of Computational Fluid Dynamics 1998*, edited by D. A. Caughey and M. M. Hafez, World Scientific, New York, 1998, pp. 363–380.

[10]Obayashi, S., and Takanashi, S., "Genetic Optimization of Target Pressure Distribution for Inverse Design Methods," AIAA Paper 95-1649, 1995.

[11]Kim, H. J., and Rho, O.-H., "Dual-Point Design of Transonic Airfoils Using the Hybrid Inverse Optimization Method," *Journal of Aircraft*, Vol. 34, No. 5, 1997, pp. 612–618.

[12]Tan, C. S., Hawthorne, W. R., McCune, J. E., and Wang, C., "Theory of Blade Design for Large Deflections, Part II: Two-Dimensional Cascades," *Journal of Engineering for Gas Turbines and Power*, Vol. 106, No. 2, 1984, pp. 354–365.

[13]Leonard, O., and Van den Braembussche, R. A., "Design Method for Subsonic and Transonic Cascade with Prescribed Mach Number Distribution," *Journal of Turbomachinery*, Vol. 114, No. 3, 1992, pp. 553–560.

[14]Tong, S. S., and Thompkins, W. T., "A Design Calculation Procedure for Shock-Free or Strong Passage Shock Turbomachinery Cascades," *Journal of Engineering for Power*, Vol. 105, No. 2, 1983, pp. 369–376.

[15]Dang, T. Q., Nerurkar, A. C., and Reddy, D. R., "Design Modification of Rotor 67 by 3D Inverse Method–Inviscid Flow Limit," American Society of Mechanical Engineers Paper 97-GT-484, 1997.

[16]Dulikravich, G. S., and Sobieczky, H., "Shockless Design and Analysis of Transonic Cascade Shapes," *AIAA Journal*, Vol. 20, No. 11, 1982, pp. 1578–1582.

[17]Sanz, J. M., "Improved Design of Subcritical and Supercritical Cascades Using Complex Characteristics and Boundary-Layer Correction," *AIAA Journal*, Vol. 22, No. 7, 1984, pp. 950–956.

[18]Dang, T. Q., and Isgro, V., "Euler-Based Inverse Method for Turbomachinery Blades: Part I, Two-Dimensional Cascades," *AIAA Journal*, Vol. 33, No. 12, 1995, pp. 2309–2315.

[19]Jameson, A., Schmidt, W., and Turkel, E., "Numerical Solutions of the Euler Equations by Finite Volume Methods Using Runga–Kutta Time-Stepping Schemes," AIAA Paper 81-1259, 1981.

[20]Jameson, A., "Transonic Flow Calculations for Aircraft," *Lecture Notes in Mathematics,* edited by F. Brezzi, Vol. 1127, Springer-Verlag, New York, 1985, pp. 156–242.

[21]Pulliam, T. H., "Artificial Dissipation Models for the Euler Equations," AIAA Paper 85-0438, 1985.

[22]Yokota, J. W., "Vorticity Dynamics of Inviscid Shear Layers," *AIAA Journal*, Vol. 31, No. 8, 1993, pp. 1430–1439.

[23]Yokota, J. W., "A Kinematic Velocity Decomposition of Stratified Flow," *International Journal of Computational Fluid Dynamics*, Vol. 9, 1998, pp. 121–135.

[24]Goldstein, M. E., *Aeroacoustic*, McGraw–Hill, New York, 1976, pp. 44, 45.

[25]Yokota, J. W., "Potential/Complex-Lamellar Descriptions of Incompressible Viscous Flow," *Physics of Fluids*, Vol. 9, No. 8, 1997, pp. 2264–2272.

[26]Yokota, J. W., "Unsteady Vortex–Blade Row Interactions," *CASI Journal*, Canadian Aeronautics and Space Inst., Vol. 44, No. 1, 1998, pp. 25–32.

[27]Denton, J. D., "The Use of a Distributed Body Force to Simulate Viscous Effects in 3D Flow Calculations," American Society of Mechanical Engineers Paper 86-GT-144, 1986.

[28]Adamczyk, J. J., Mulac, R. A., and Celestina, M. L., "A Model for Closing the Inviscid Form of the Average Passage Equation System," American Society of Mechanical Engineers Paper 86-GT-227, 1986.

[29]Adamczyk, J. J., Celestina, M. L., Beach, T. A., and Barnett, M., "Simulation of 3-D Viscous Flow Within a Multi-Stage Turbine," *Journal of Turbomachinery*, Vol. 112, 1989, pp. 370–376.

[30]Yokota, J. W., and Medd, A. J., "Convergence Acceleration of an Inverse Design Technique for Constructing Turbomachinery Cascades," *AIAA Journal*, Vol. 38, No. 10 , 2000, pp. 1983–1985.